Parametric studies of aerofoil-vortex interaction; a numerical approach using LES

M. Ilie
marcel.Ilie@ucf.edu
University of Central Florida
Orlando, Florida
USA

F. Nitzsche and E. Matida
Carleton University
Ottawa
Canada

ABSTRACT

The influence of angle-of-attack and vortex-aerofoil vertical miss-distance on the aerofoil-vortex mechanism of interaction is investigated numerically using the large-eddy simulation approach. The study concerns the aerofoil-vortex interaction (AVI) phenomena encountered in the rotorcraft aerodynamics. The studies are performed for a Reynolds number of $1{\cdot}3 \times 10^6$ based on the chord (c = 0·2m) of the aerofoil and free-stream velocity U = 100ms^{-1}. The studies are conducted for three different angles-of-attack (α = 0°, and α = 5°, α = 10°) and vertical miss-distances (h = 0·0m, h = –0·01, h = –0·02m) respectively. The present study shows that the magnitude of lift coefficient and flow separation, at the instant of interaction, decay with the increase of angle-of-attack and vertical miss-distance.

NOMENCLATURE

C_p	pressure coefficient
C_l	lift coefficient
C_s	Smagorinsky constant
c	chord of aerofoil
D_{wall}	van Driest wall damping function
T	time step
h	vortex-aerofoil vertical miss distance
v_T	subgrid scale viscosity
τ_{ij}	subgrid scale tensor

1.0 INTRODUCTION

During certain rotorcraft flight-conditions (mainly descent or extreme manoeuvres), vortices generated at the tip of the rotor blade interact with the next advancing blade, generating the so-called blade-vortex interaction (BVI) phenomenon. The BVI phenomenon is a major source of undesired acoustic noise and vibration in rotorcraft. Thus, there is a high interest in the rotorcraft industry to understand the BVI phenomenon to reduce the noise and vibrations associated with it. Strong BVIs are normally caused by vortices with an axis that is parallel (or nearly parallel) to the spanwise axis of the blade, as shown in Fig. 1. For the past decades, the BVI phenomenon has been investigated both experimentally and numerically[1-8].

Previous experimental studies concerned the measurement of incompressible (Mach number, Ma = 0·17) BVI pressure data in a wind tunnel[1]. Some other experimental studies concerned the AVI measurements of lift, drag, and moment coefficients over an aerofoil at zero angle-of-attack[2]. In this study hot-wire measurements were conducted to determine the vortex velocity distribution. The generation of a single vortex in AVI measurements is challenging, and most

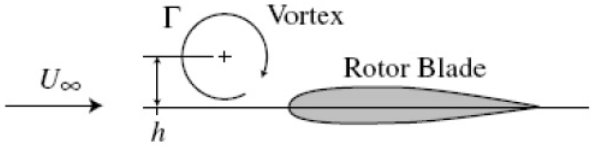


Figure 1. Schematic view of blade-vortex interaction.

Paper No. 3646. Manuscript received 11 November 2010, revised version received 14 March 2011, accepted 19 October 2011.

https://doi.org/10.1017/S0001924000006424 Published online by Cambridge University Press

of the experiments have relied upon pitching aerofoils to create vortices, which would be advected and interact with a fixed aerofoil[1-2]. Experimental studies have indicated that the unsteady lift depends on vortex strength, vortex core size, blade-vortex vertical miss-distance (indicated as '*h*' in Fig. 1), and the aerofoil angle-of-attack[4, 5].

The first numerical investigations of BVI were based on the inviscid flow theory (panel methods or simulations using the Euler system of equations), which presents the shortcoming of not being able to provide drag coefficients directly neither handling flow separation[2,3]. A discrete free-vortex method was used to obtain lift and moment coefficients for different vortex miss-distances, vortex strengths, and aerofoil angle-of-attack. Lagrangian vortex methods were also used in the study of BVIs[6]. Recent developments of the computational systems made the use of Computational-Fluid Dynamics (CFD) more feasible. However, the CFD techniques present certain limitations associated with the turbulence modeling, time-dependent solutions and computational costs respectively. Thus, the Reynolds-Averaged Navier-Stokes (RANS) technique is not suitable for time-dependent problems. On the other-hand the unsteady Reynolds-Averaged Navier-Stokes (URANS) presents certain limitations associated with the turbulence modeling. Previous CFD studies identified the dissipative nature of URANS[8-9]. Recently, numerical studies have employed the hybrid RANS/LES method (with a RANS zone around the aerofoil and the aerofoil wake region along with LES outside this zone) to study AVI[10]. Direct Numerical Simulations (DNS) is the most accurate method to obtain the flow solution. However, due to the grid resolution requirements, proportional to $R_e^{9/4}$, DNS is limited to low-Reynolds number flows, about R_e = 10,000. Thus, to circumvent the limitations posed by these CFD approaches, in the present work we employ the large-eddy simulation (LES) approach for the numerical investigation of AVI.

It is worth to notice that although LES is computationally less expensive than DNS; LES is still a lot more expensive than URANS, when memory and processing time are considered. Similar to DNS, LES provides a time dependent solution of the Navier-Stokes equations. In LES, the more energetic large scales of turbulence are resolved, but the more homogenous and small scales of turbulence are eliminated (through a proper low-passing filtering procedure) and their contribution has to be modelled. The standard LES Smagorinsky-Lilly model with the van Driest damping function is adopted here to investigate the effect of the angle-of-attack on AVIs[11,12]. Drag and lift coefficients, as function of time for different vertical miss-distances and angle of attack, were computed.

2.0 COMPUTATIONAL METHOD

As already stated in the present study the LES approach is used for the numerical computations of AVI. For the solution of the filtered Navier-Stokes equations, a second-order central-difference scheme is used. For the time advancement, a second-order accurate implementation using a backward implicit difference formula is used. No forcing is added on the computational domain. The filtered Navier-Stokes equations are:

$$\frac{\partial \bar{u}_i}{\partial x_i} = 0 \qquad \ldots (1)$$

$$\frac{\partial \bar{u}_i}{\partial t} + \frac{\partial}{\partial x_j}\left(\bar{u}_i \bar{u}_j\right) = -\frac{\partial \bar{p}}{\partial x_i} - \frac{\partial \tau_{ij}}{\partial x_j} + \frac{1}{\mathrm{Re}}\frac{\partial^2 \bar{u}_i}{\partial x_j \partial x_j} \qquad \ldots (2)$$

where is the subgrid scale (SGS) given by:

$$\tau_{ij} = \overline{u_i u_j} - \bar{u}_i \bar{u}_j \qquad \ldots (3)$$

and is modeled. In the present work the SGS proposed by Smagorinsky and Lilly[9,10] is used. The SGS stresses are related to the strain rate tensor by SGS viscosity, v_T;

$$\tau_{ij} - \frac{1}{3}\delta_{ij}\tau_{kk} = 2\nu_T \bar{S}_{ij} \qquad \ldots (4)$$

The SGS viscosity v_T is given by:

$$\nu_T = \rho(C_s D_{wall}\Delta)^2 \left|\bar{S}\right| \qquad \ldots (5)$$

where C_s is the Smagorinsky constant (C_s = 0·1 in the present work), D_{wall} represents the van Driest wall damping factor, Δ is the filter width and $\left|\bar{S}\right|$ represents the magnitude of the large-scale strain-rate tensor.

$$\bar{S}_{ij} = \frac{1}{2}\left(\frac{\partial \bar{u}_i}{\partial x_j} + \frac{\partial \bar{u}_j}{\partial x_j}\right) \qquad \ldots (6)$$

More complex SGS models have appeared in the literature, for example the dynamic SGS eddy viscosity models[13], but they are beyond the scope of the present work.

Quasi 3D simulations (spanwise direction $z = 1c$) were performed for a Reynolds number, Re = 1·3 × 10^6, based on the free stream velocity, U_∞ = 100ms^{-1}, and the chord of a NACA 0012 aerofoil, c = 0·2m, at the limit of incompressibility for Mach number, Ma = 0·3. The aerofoil was centred in the computational domain, which consists of a rectangular block with the sides equal to 9c and a spanwise size of 1c. For computational efficiency reasons, the computational domain was divided into 12 blocks as presented in Fig. 2. Parallel processing, using MPI, was employed.

The computational domain consists of approximately 12.6 million structure grid points with a cluster of grid points around the aerofoil and a grid expansion factor of 0·5. For all the computations in the present analysis, a time step of 1 × 10^{-6} seconds was chosen, maintaining a Courant–Friedrichs–Lewy (CFL) number smaller than unity throughout the domain and the entire simulation. Ilie (2009) performed a grid convergence analysis, using a finer grid having approximately a double number of grid points, and found identical results for the lift coefficient variation as function of time (for 0° angle-of-attack), indicating that the adopted gird size is adequate for LES when the aerodynamic coefficients are of concern[16].

The core size of the vortex was set equal to c/4, where c is the chord of the aerofoil and the strength of the vortex provides a 25% higher velocity than the uniform free-stream velocity. The size of the vortex core is based on the most critical scenario of BVI phenomena[16]. Vertical miss-distances, h (as shown in Fig. 1), varying from h = 0·0 to –0·02m were investigated. For all test cases, the releasing location of the vortex is x = 0·13m upstream of the leading edge. The release location of the vortex was based on computational reasons[17].

No slip boundary conditions were used at the aerofoil wall. A constant velocity condition (100ms^{-1}) was used at the inlet-surface. Free slip boundary conditions were used at the top and bottom surfaces of the domain, symmetry boundaries at the side surfaces, and opening boundary at the right end of the computational domain. A cluster of computers having 128 CPUs and 2GB memory per processor is used in the simulations. The lift coefficient is defined as:

$$c_l = \frac{L'}{\frac{1}{2}\rho_\infty V_\infty^2 c} \qquad \ldots (7)$$

where L' is the lift force per unit span and c is the characteristic chord length. The drag coefficient is defined as:

$$c_d = \frac{D'}{\frac{1}{2}\rho_\infty V_\infty^2 c} \qquad \ldots (8)$$

where D' is the drag force per unit span.

https://doi.org/10.1017/S0001924000006424 Published online by Cambridge University Press

3.0 RESULTS AND DISCUSSION

The numerical computations were performed in the following sequence:
(1) First the flow field for the case of uniform flow past the aerofoil was solved using the Reynolds-averaged Navier-Stokes equations using a shear stress transport (SST) turbulence model by Menter[14]; (2) Second, the LES simulation for the case of uniform flow past the aerofoil was initialised using the RANS solution results; (3) Once the flow was fully developed, the LES (typically after 10,000 time steps) solution results are collected and used for the initialisation of vortex superimposed on a uniform flow. The vortex equation was based on Bossel[15]. The present study is based on the recent computational investigation of BVI[17].

Figure 3 shows the instantaneous magnitude of velocities, from the final LES solution, in the near field of the aerofoil (see Fig. 2 for the size of the whole computational domain). It is worth to mention that all the important aerodynamics occurs in the near-field region of the aerofoil. The reason for a larger domain is based on the aeroacoustics considerations were the near-wall effect should be avoided[18,19].

The results are presented for an angle-of-attack $\alpha = 0°$, at five different instants in time as a clockwise rotating vortex travels from the releasing point at three different vertical miss distances, $h = 0{\cdot}00$ m, $h = -0{\cdot}01$m, and $h = -0{\cdot}02$m, respectively. Following the trajectory for $h = 0{\cdot}00$m, the clockwise vortex was released upstream of the aerofoil ($x = 0{\cdot}13$m). While traveling towards the aerofoil, the

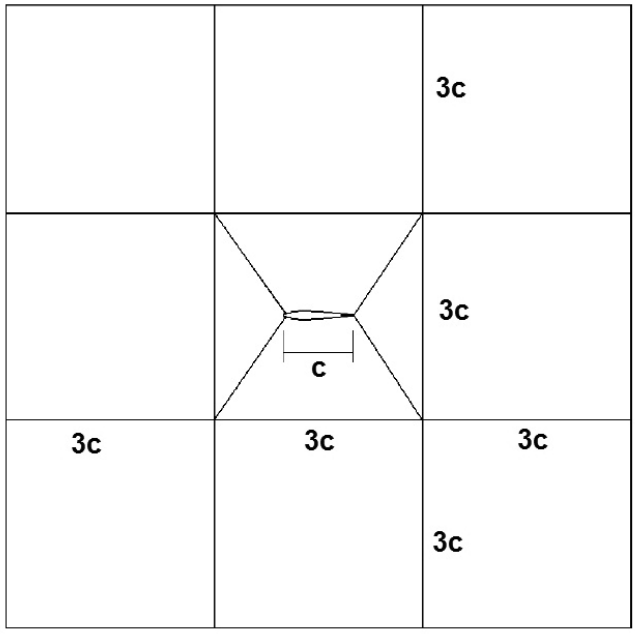


Figure 2. Multi-block domain for the aerofoil (NACA0012) at 0° angle-of-attack (0·1*c* perpendicular to the figure).

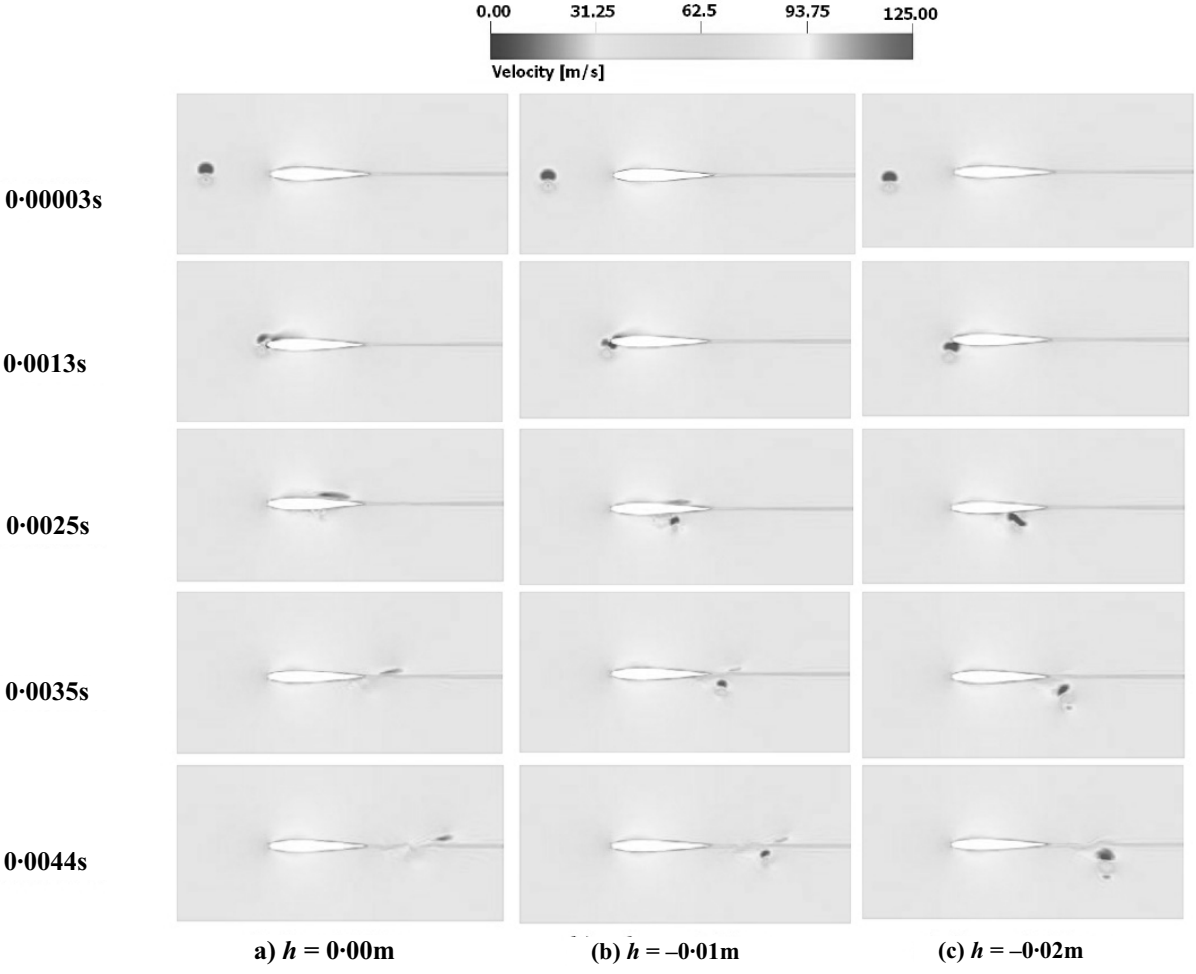


Figure 3. Time evolved fluid structures (velocity magnitude), angle-of-attack $\alpha = 0°$.

https://doi.org/10.1017/S0001924000006424 Published online by Cambridge University Press

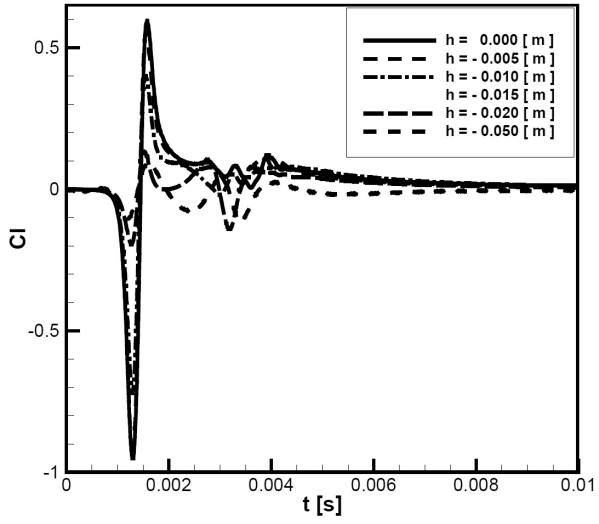


Figure 4. Comparison of lift coefficient, $\alpha = 0°$.

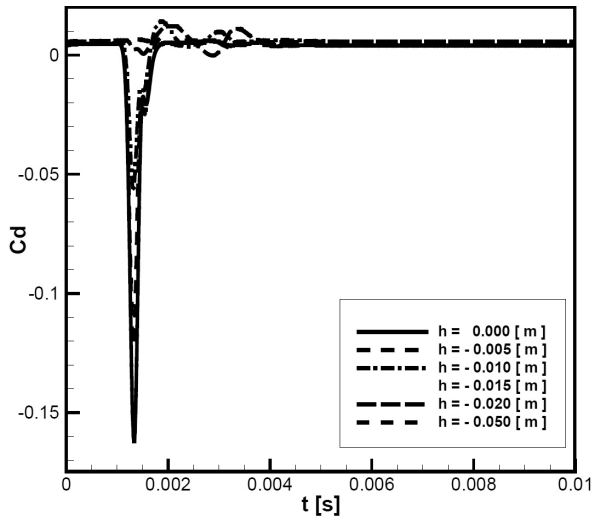


Figure 5. Time history of drag coefficient, $\alpha = 0°$.

vortex induces a velocity, pointing downward, on the aerofoil. This will change the effective angle of attack (pointing downwards), thus generating negative lift. At the instant of interaction (about t = 0·0013s), the balance of pressure at the upper and lower surface of the aerofoil is altered. Consequently, higher velocity is observed at the upper surface of the aerofoil while the velocity exhibits lower values underneath of aerofoil. This sudden change in velocity field corresponds to a sudden change in pressure field, which in turn causes a sudden change in lift coefficient. The vortex-aerofoil mechanism of interaction causes a significant distortion of the vortex, as seen in Fig. 3, at instant t = 0·0035s.

Increasing the miss-distances, h = –0·01 and –0·02m, the vortex-aerofoil interactions are less significant and both the vortex induced velocity and the sudden change in lift coefficient decay. The time history of velocity magnitude reveals that with the increase of the vertical miss-distance the vortex interacts less with the upper surface and progressively more with the lower surface of the aerofoil, influencing the vortex-aerofoil mechanism of interaction. This is best illustrated in Fig. 2, for case of h = –0·02m, at instant t = 0·0044s. As a result of the vortex-aerofoil mechanism of interaction two counter-rotating vortices are generated.

Figures 4 and 5 show the comparison of lift and the drag coefficients, respectively, for three different values of vertical miss-distance, h = 0·0, –0·01, and –0·02m. As discussed above, as the vortex approaches the aerofoil it generates a negative lift which reaches a minimum at instant t = 0·0013s (when the center of the vortex is near the leading edge of the aerofoil) for all miss-distances, as shown in Fig. 4. The decay of lift coefficient is followed by a sudden jump to a maximum value. The magnitude difference between the minimum and the maximum lift coefficient, normally referred to as the 'incremental lift coefficient', is inversely proportional to the miss-distance, i.e., larger miss-distances produce smaller incremental lift coefficients. After the maximum is achieved, the lift coefficient decreases gradually as the vortex interacts with the aerofoil.

For h = 0·00m, when the residual component of the vortex approaches the trailing edge and about to leave the aerofoil, the lift coefficient increases, reaches a local maximum (when part of the upper-half vortex starts to leave the aerofoil), decreases to a local minimum (when the lower-half of the vortex has completely left the aerofoil) and changes to another local maximum (the remainder of the vortex induces a velocity pointing upward on the aerofoil) before asymptotically going to zero while the distorted vortex travels downstream of the aerofoil. It is worth to notice a more pronounced lift coefficient variation when the vortex is leaving the aerofoil for h = –0·02m, after interacting more with the lower surface of the aerofoil (higher velocities producing lower localised pressures at the lower surface of aerofoil).

In Fig. 5, for all miss-distances, the drag coefficient becomes negative as the vortex is approaching the aerofoil, reaches a minimum value, which is inversely proportional to the miss-distances. There is also considerable variation in drag coefficients while the distorted vortex is leaving the aerofoil. This variation is more pronounced for larger miss-distances. The negative values of lift coefficient are associated with the flow separation and reverse flow. The reverse flow causes an acceleration of the blade. Thus, as the vortex interacts with the aerofoil the blade is subjected to a lead-lag motion which is partially responsible for the vibrations induced to the rotor hub[16].

The second study concerns the influence of angle-of-attack on the vortex-aerofoil mechanism of interaction. Thus, similar study was conducted for an aerofoil at angle of attack $\alpha = 5°$ and the results are presented in Figs 6, 7 and 8. Figure 6 presents the velocity magnitude for three different miss-distances, h = 0·0, –0·01, –0·02m. In spite of an overall similarity to angle-of-attack = 0°, there are subtle differences. There is a more pronounced separation bubble formation when the residual component of the vortex interacts with the upper-surface of aerofoil (for h = 0·0 and –0·01m) and the 'dual-core' vortices for h = –0·01 and –0·02 m have less strength when compared against similar cases for = 5°. The incremental lift coefficient decreases when the miss-distance increases, as shown in Fig. 7, while the variations of the lift coefficient when the vortex leaves the aerofoil are more pronounced for h = 0·00 m when compared against the case for $\alpha = 0°$ as shown in Fig. 4 (h = 0·00m).

Figure 8 shows that the drag coefficient increases, as the vortex approaches the aerofoil at $\alpha = 5°$, reaching a maximum before dropping drastically. Minimum values of drag coefficient are observed at approximately t = 0·0013 and 0·0015s, followed by a sequence of fluctuations, as the distorted vortex is departing from the aerofoil. The increase in angle-of-attack generates large fluctuations of the lift coefficient as the vortex departures the aerofoil, for h = 0·00m.

Figure 9 presents the instantaneous magnitude of velocities for an angle of attack $\alpha = 10°$, at five different instants in time, as a clockwise rotating vortex travels at three different vertical miss distances h = 0·00 m, h = –0·01m and h = –0·02m. Similar to the test cases $\alpha = 0°$ and $\alpha = 5°$, it is observed that the vortex-aerofoil vertical miss distance influences the mechanism of interaction in a particular manner. Hence, for the case of a vertical miss distance h = 0·00m, the vortex-aerofoil interaction is severe and the vortex is significantly distorted.

https://doi.org/10.1017/S0001924000006424 Published online by Cambridge University Press

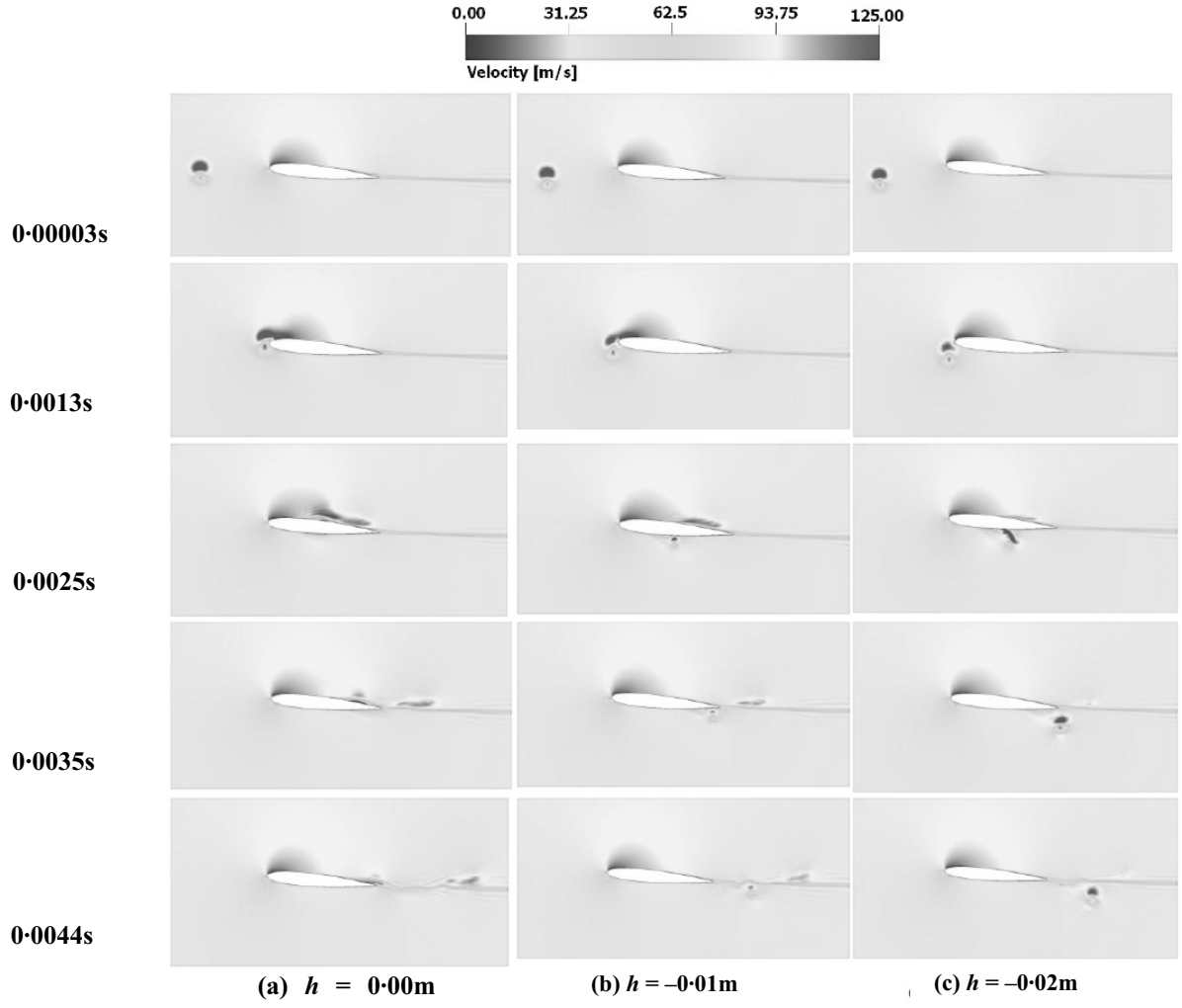


Figure 6. Time evolved fluid structures (velocity magnitude), angle-of-attack α = 5°.

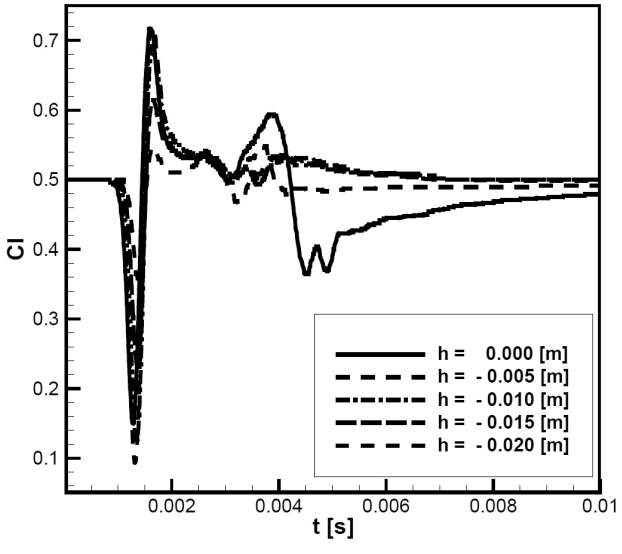


Figure 7. Comparison of lift coefficient, α = 5°.

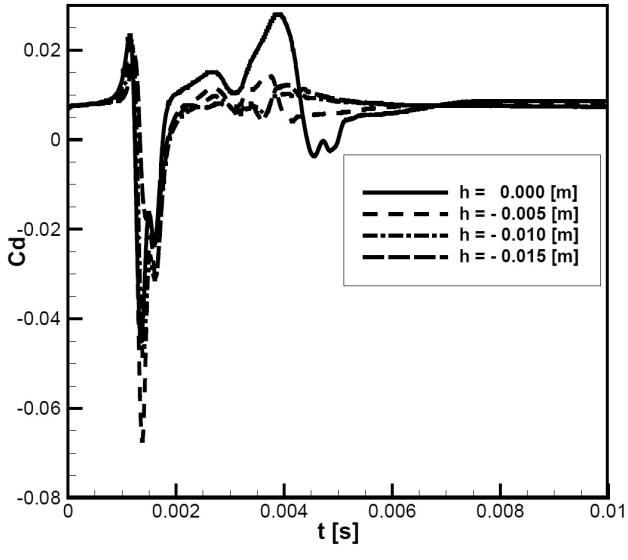


Figure 8. Comparison of drag coefficient, α = 5°.

https://doi.org/10.1017/S0001924000006424 Published online by Cambridge University Press

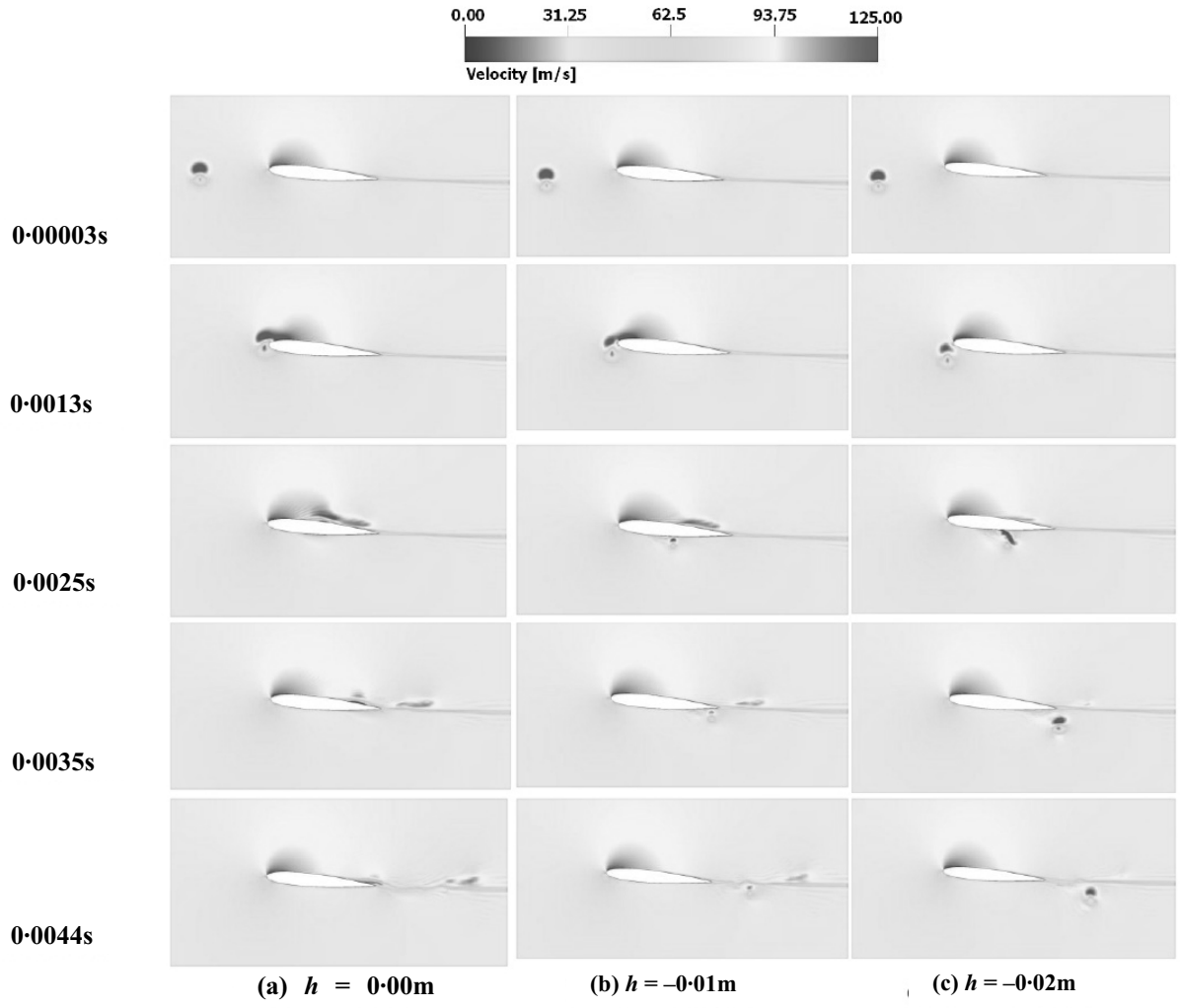


Figure 9. Time evolved fluid structures (velocity magnitude), angle-of-attack α = 10°.

The vortex-aerofoil mechanism of interaction, for a vertical miss distance h = 0·00m, is associated with the distortion of the vortex and increase of velocity. Large flow separation is observed at the upper surface of aerofoil as seen in Fig. 9(a). For the test case of a vertical miss distance h = 0·00m, the vortex splits into two residual components, one traveling above the aerofoil and the other one traveling underneath the aerofoil. The residual component of the vortex, which travels underneath the aerofoil, exhibits a smaller core size and a weaker strength than the one that travels above the aerofoil. As the two residual components of the vortex travel downstream the aerofoil, they merge into the aerofoil wake and disturb it. As a result of the merging process, the two residual components of the vortex dissipate as they travel far downstream the aerofoil.

With the increase of vertical miss distance, it is observed that the vortex slides underneath of aerofoil and the vortex-aerofoil interactions are less sever. For the case of a vertical miss distance h = –0·01m, the vortex still splits into two residual components. In this case, the residual component of the vortex that travels underneath the aerofoil presents a larger core size and a higher strength than the one that travels above the aerofoil. A direct comparison of the velocity field for angles-of-attack α = 5° and α = 10°, at instant t = 0·0035s, Fig. 6(b) and Fig. 9(b), reveals the fact that the angle-of-attack influences the vortex-aerofoil mechanism of interaction in a particular manner.

Thus, for an angle of attack α = 10°, the residual component of the vortex that travels underneath of aerofoil exhibits a larger core size and strength than the one corresponding to an angle of attack α = 5°, as seen in Figs 9(b) and respectively 6(b), at instant t = 0·0035s. As the residual component of the vortex travels downstream the aerofoil, it dissipates and large disturbances of the aerofoil wake are observed, Fig. 9(b), t = 0·0044s.

Increasing the vertical miss distance to h = –0·02m, the vortex-aerofoil interaction is less severe and the vortex preserves better its characteristics (strength and core size) as seen in Fig. 9(c). This can be better quantified by a direct comparison of test cases h = –0·01m and h = –0·02m, Figs 9(b) and 9(c), at instant t = 0·0025s.

Also a direct comparison of the time-dependent velocity, at the instant t = 0·0035s, reveals important aspects of the flow physics. It is apparent that for the test case h = –0·02m, the vortex core is highly distorted when compared with the test case h = –0·01m. However, as the time elapses, the residual component of the vortex, due to its own inertia, restores its characteristics, redefining a distinctive vortex, as seen in Fig. 9(c) at the instant t = 0·0044s.

As the residual component of the vortex travels downstream the aerofoil, merges with the aerofoil wake and alters it. The disturbances of the wake are reflected into the fluctuations of the aerodynamic coefficients as seen in Figs 10 and 11 respectively.

Figure 10 presents the comparison of lift coefficient for different vortex-aerofoil vertical miss distances. The aerodynamic coefficients, for angle-of-attack α = 10°, present similar behaviour with the ones observed for angles-of-attack α = 0° and α = 5°. The comparison reveals that the amplitudes of lift coefficient, at the instant when the vortex encounters the aerofoil, t = 0·0013s, decrease with the increase of vertical miss distance.

https://doi.org/10.1017/S0001924000006424 Published online by Cambridge University Press

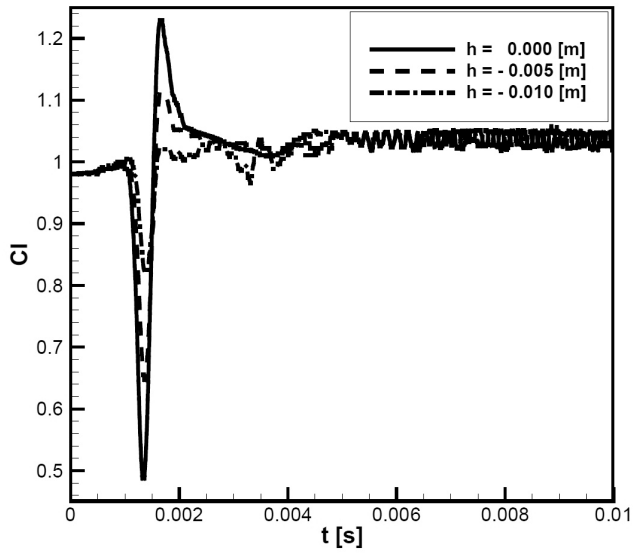


Figure 10. Comparison of lift coefficient, $\alpha = 10°$.

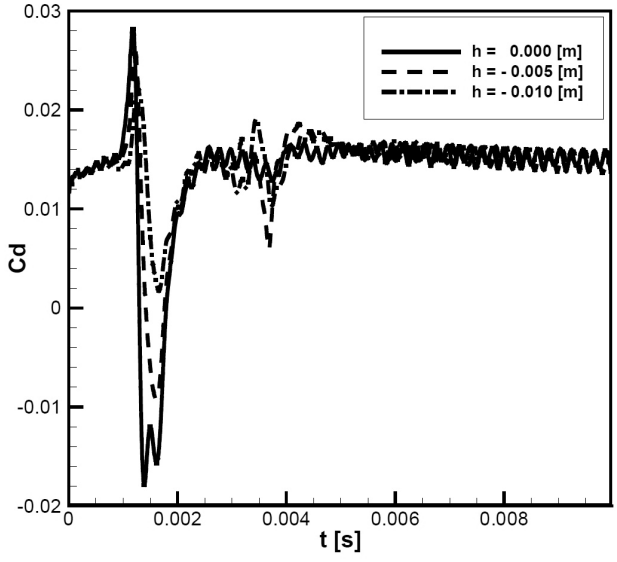


Figure 11. Comparison of drag coefficient, $\alpha = 10°$.

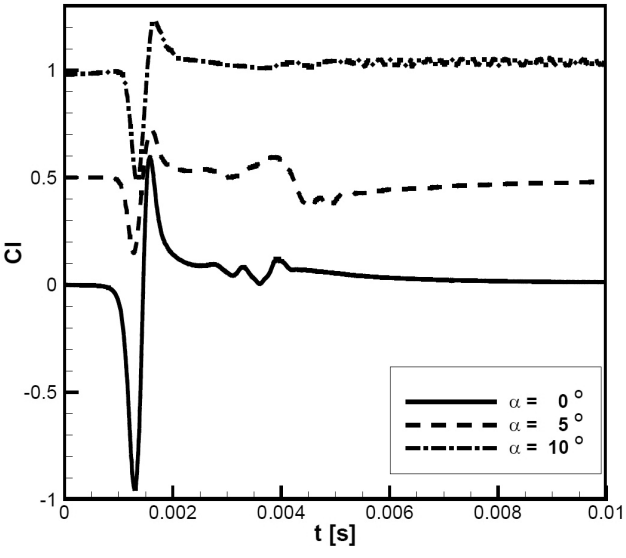


Figure 12. Comparison of lift coefficient, $h = 0{\cdot}000$m.

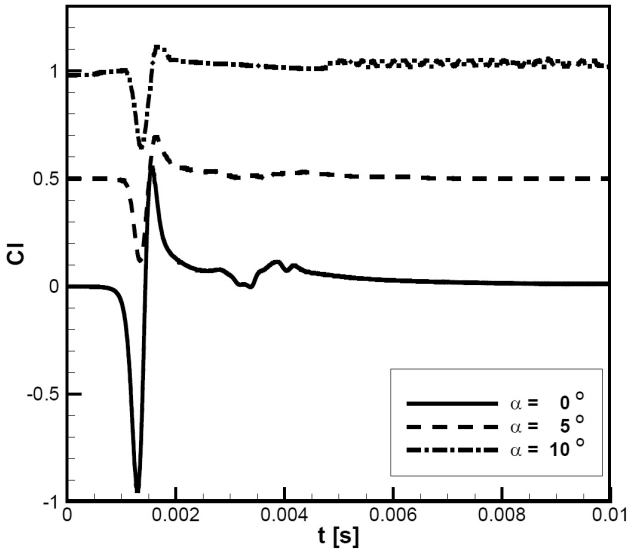


Figure 13. Comparison of lift coefficient, $h = -0{\cdot}005$m.

Also, as the vortex-aerofoil vertical miss distance increases, larger fluctuations of lift coefficient are present at the instant when the residual component of the vortex travels the chord length of aerofoil. This is best illustrated for a vertical miss distance $h = -0{\cdot}01$m, Fig. 10. As the residual component of the vortex travels far downstream the aerofoil, the lift coefficient presents similar behaviour for all vertical miss distances.

The fluctuations of lift coefficient, at the instant when the residual component of the vortex leaves the aerofoil $t = 0{\cdot}0035$s, are still present for angle-of-attack $\alpha = 10°$, as observed in Fig. 10· The disturbances of the wake are reflected into the fluctuations of lift coefficient, after the instant $t = 0{\cdot}005$s.

The drag coefficient, for angle-of-attack $\alpha = 10°$, follows similar trend as seen for angles-of-attack $\alpha = 0°$ and $\alpha = 5°$ respectively. Thus, the vortex-aerofoil mechanism of interaction is associated with flow separation, and reverse flow, indicated by the negative values of drag coefficient. A decay of the amplitudes of drag coefficient, at the instant when the vortex encounters the aerofoil, is observed as the vertical miss distance increases. Also, the amount of reverse flow decreases with the increase of vortex-aerofoil vertical miss distance. Thus, no reverse flow is observed for a vertical miss distance $h = -0{\cdot}01$m. However, an increase of the fluctuations of drag coefficient is observed with the increase of vertical miss distance. This is best illustrated in Fig. 11, at the instant $t = 0{\cdot}0035$s. This behaviour of the time-dependent drag coefficient is a result of the vortex-aerofoil mechanism of interaction as well.

Figure 12 presents the comparison of lift coefficient for three angles-of-attack, $\alpha = 0°$, $\alpha = 5°$ and $\alpha = 10°$ respectively, for a vortex-aerofoil vertical miss distance $h = 0{\cdot}00$m. The comparison shows a decay of the amplitude of the lift jump, at the instant when the vortex encounters the aerofoil, with the increase of angle-of-attack.

Large fluctuations of lift coefficient are observed for an angle-of-attack $\alpha = 5°$, at the instant when the residual component of the vortex leaves the aerofoil. These fluctuations are due to the

https://doi.org/10.1017/S0001924000006424 Published online by Cambridge University Press

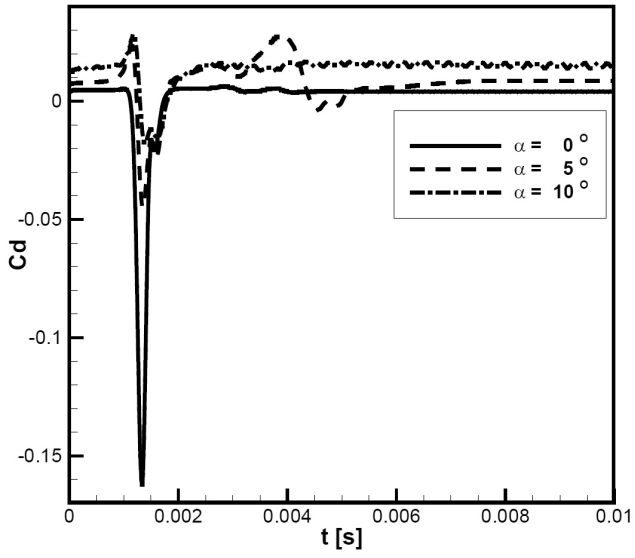


Figure 14. Comparison of drag coefficient, h = 0·000m.

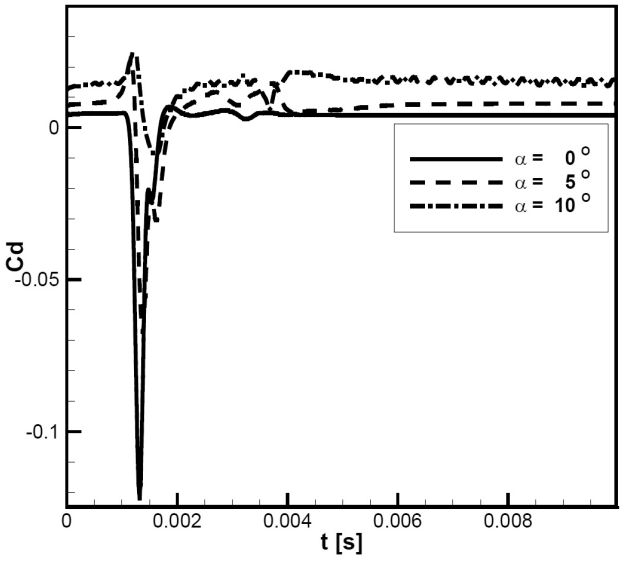


Figure 15. Comparison of drag coefficient, h = –0·005m.

influence of angle of attack on the vortex-aerofoil mechanism of interaction. Also for the angles-of-attack $\alpha = 0°$ and $\alpha = 5°$, the lift coefficient presents differences at the instants when the residual component of the vortex leaves the aerofoil. Hence, for an angle-of-attack $\alpha = 0°$, the lift coefficient converges to a constant value by an asymptotic decay, while for an angle of attack $\alpha = 5°$, the lift coefficient converges to a constant value by an asymptotic growth. For an angle-of-attack $\alpha = 10°$, the fluctuations of lift coefficient at the instant when the residual component of the vortex leaves the aerofoil are less significant.

Similar behaviour of lift coefficient was observed for larger values of vertical miss distance. However, a decay of lift fluctuations was observed at the instant when the residual component of the vortex leaves the aerofoil, Fig. 13, t = 0·0035s. Independent of angle-of-attack and vortex-aerofoil vertical miss distance as the residual component of the vortex travels far downstream the aerofoil, the lift coefficient converges to a constant value corresponding to the case of uniform flow past NACA 0012, at the angles-of-attack $\alpha = 0°$, $\alpha = 5°$ and $\alpha = 10°$ respectively.

Figure 14 presents the comparison of the time-dependent drag coefficient, for three different angles-of-attack, for a vortex-aerofoil vertical miss distance h = 0·00m. The comparison reveals that the amplitudes of drag coefficient, at the instant of interaction, decay with the increase of angle-of-attack. Also the amount of reverse flow decays with the increase of angle-of-attack. Similar to lift coefficient behaviour, large fluctuations of drag coefficient are observed for an angle-of-attack $\alpha = 5°$, at the instant when the residual component of the vortex leaves the aerofoil, t = 0·0035s. These are also consequences of the influence of angle-of-attack on the vortex-aerofoil mechanism of interaction. Increasing the vortex-aerofoil vertical miss distance, to h = –0·005m, relatively large fluctuations of drag coefficient are observed for angles-of-attack $\alpha = 5°$ and $\alpha = 10°$, at the instant when the residual component of the vortex leaves the aerofoil, Fig. 15, instant t = 0·0035s. The analysis of drag coefficient shows that with the increase of vortex-aerofoil vertical miss distance, the amplitudes of drag coefficient, at the instant when the vortex encounters the aerofoil t = 0·0013s, decays.

The study also shows that for all three angles-of-attack $\alpha = 0°$, $\alpha = 5°$ and $\alpha = 10°$, as the residual component of the vortex travels far downstream the aerofoil; it merges into the wake and dissipates, causing the convergence of drag coefficient to a constant value.

4.0 CONCLUSIONS

Parametric investigations based on the aerofoil angle-of-attack and vortex-aerofoil vertical miss distance were conducted to investigate their influence on the unsteady pressure field about a NACA 0012 aerofoil, for a Reynolds number Re = 1·3 × 10^6, using LES. The vortex was released upstream of aerofoil and the unsteady flow field results were stored at regular time intervals, corresponding to different vortex core locations, along the vortex trajectory and were used for the calculation of the aerodynamic coefficients.

Calculations were made for three different BVI problems based on the aerofoil angle-of-attack $\alpha = 0°$, $\alpha = 5°$ and $\alpha = 10°$ respectively, with varying the vortex-aerofoil miss-distances. The presence of the vortex in the flow field induces a velocity at the surface of aerofoil, generating a time-varying lift and drag coefficient. The variation of the aerodynamic coefficients depends on the vortex-aerofoil mechanism of interaction, defined by aerofoil angle-of-attack and vortex-aerofoil vertical miss distance. For small vertical miss distance values, the vortex–aerofoil mechanism of interaction is associated with flow separation and reverse flow.

REFERENCES

1. HORNER, M.B. SALIVEROS, E. KOKKALIS, A. and MCD. GALBRAITH, R.A. Results from a set of low speed blade-vortex interaction experiments, *Experiments in Fluids*, 1993, **14**, pp 341-352.
2. STRAUS, J., RENZONI, P. and MAYLE, R.E. Airfoil Pressure Measurements During a Blade Vortex Interaction and a Comparison with Theory, *AIAA J*, 1990, **28**, (2), pp 222-228.
3. RENZONI, P. and MAYLE, R.E. Incremental force and moment coefficients for a parallel blade-vortex Interaction, *AIAA J*, 1991, **29**, (1), pp 6-13.
4. ABELLÓ, J.C. and GEORGE, A.R. Rotorcraft BVI noise reduction by attitude modification. In: Paper presented at the 5th AIAA/CEAS aeroacoustics conference, Bellevue, Washington, USA, 10–12 May 1999.
5. ABELLO, J. and GEORGE, A. Wake displacement study of attitude and flight parameter modifications to reduce rotorcraft blade–vortex interaction (BVI) noise. In: Ninth AIAA/CEAS aeroacoustics conference, Hilton Head, SC; 12–14 May 2003.
6. OPOKU, D.G., TRIANTOS, D.G., NITZSCHE, F. and VOUTSINAS, S.G. Rotorcraft Aerodynamic and Aeroacoustic Modelling Using Vortex Particle Methods. ICAS Paper No. 2002-299, 2002.

https://doi.org/10.1017/S0001924000006424 Published online by Cambridge University Press

7. WONG, A., NITZSCHE, F. and KHALID, M. Formulation of Reduced-Order Models for Blade-Vortex Interactions Using Modified Volterra Kernels, Paper No. 7, Proceedings: 30th European Rotorcraft Forum, 14-16 September 2004, Marseilles, France.
8. NAGARAJAN, S. and LELE, S. Prediction of Sound Generated by a Pitching Airfoil: A comparison of RANS and LES, 12th AIAA/CEAS Aeroacoustics Conference, 8-10 May 2006, Cambridge, MA, USA.
9. LARDEAU, S. and LESCHZINER, M.A. Unsteady Reynolds-averaged Navier-Stokes computations of transitional wake/blade Interaction, AIAA, 2004, **42**, (8), pp 1559-1571.
10. FELTEN, F. and LUND, T. Numerical Simulation of parallel Airfoil/Vortex Interaction Using a Zonal Hybrid RANS/LES Method, AIAA2005-5127
11. SMAGORRINSKY, J.S. General circulation experiments with the primitive equation, *Monthly Weather Rev*, 1963, **91**, pp 99-164.
12. LILLY, D.K. On the application on the eddy viscosity concept in the inertial sub-range of turbulence, 1996, NCAR Manuscript, pp 195-200.
13. GERMANO, M., PIOMELLI, U., MOIN, P. and CABOT, W.H. A dynamic subgrid-scale eddy viscosity model, *Phys Fluids A*, 1991, **3**, (7), pp 1760–1765.
14. MENTER, F.R. Two-equation eddy – viscosity turbulence models for engineering applications, 1994, *AIAA J*, **32**, (8).
15. BOSSEL, H.H. Vortex computation by the method of weighted residuals using exponentials, *J Computational Physics*, 1970, **5**, pp 359-382.
16. LEISHMAN, J.G. *Principles of Helicopter Aerodynamics*, Cambridge University Press, Cambridge, UK, 2006
17. ILIE, M. Numerical study of helicopter blade–vortex mechanism of interaction using large-eddy simulation, *Computers and Structures*, 2009, **87**, pp 758–768.
18. ILIE, M. Icing Effect on the Aeroacoustics of Helicopter Blade-Vortex Interaction: A Numerical Study Using Large-Eddy Simulation, AIAA-2010-3855, 2010
19. ILIE, M. Active Flow Control Technique for the Reduction of Helicopter BVI Noise; a Numerical Study Using Large-Eddy Simulation AIAA-2010-3871, 201.

RAeS Structures & Materials Call For Papers

3RD AIRCRAFT STRUCTURAL DESIGN CONFERENCE

ROYAL AERONAUTICAL SOCIETY

9 - 11 OCTOBER 2012 / DELFT UNIVERSITY OF TECHNOLOGY, THE NETHERLANDS

The 3rd in the series, this 3 day conference is now open for written submissions from prospective authors on a number of key topics to be discussed during the conference including;

- Structural Designs for the next generation of aircraft
- Emerging requirements for improved safety and crash worthiness
- Design with novel or advanced materials
- CRFP Structural Design for maintenance and repair
- Papers with a specific emphasis on structural mechanics can be submitted for a special Koiter session



www.aerosociety.com/events

For more details on the Call For Papers please visit the website via www.aerosociety.com/events or contact the Conference & Events Team at conference@aerosociety.com or on +44 (0)20 7670 4345.

https://doi.org/10.1017/S0001924000006424 Published online by Cambridge University Press